NJC

Accepted Manuscript

This is an *Accepted Manuscript*, which has been through the Royal Society of Chemistry peer review process and has been accepted for publication.

Accepted Manuscripts are published online shortly after acceptance, before technical editing, formatting and proof reading. Using this free service, authors can make their results available to the community, in citable form, before we publish the edited article. We will replace this *Accepted Manuscript* with the edited and formatted *Advance Article* as soon as it is available.

You can find more information about *Accepted Manuscripts* in the Information for Authors.

Please note that technical editing may introduce minor changes to the text and/or graphics, which may alter content. The journal's standard Terms & Conditions and the Ethical guidelines still apply. In no event shall the Royal Society of Chemistry be held responsible for any errors or omissions in this *Accepted Manuscript* or any consequences arising from the use of any information it contains.

ROYAL SOCIETY OF CHEMISTRY

www.rsc.org/njc

New Journal of Chemistry

ARTICLE

In-vitro Evaluation of Layered Double Hydroxide-Fe_3O_4 Magnetic Nanohybrids for Thermo-Chemo Therapy

Received 00th January 20xx,
Accepted 00th January 20xx

DOI: 10.1039/x0xx00000x

www.rsc.org/

EswaraVara Prasadarao Komarala,[a]† Saumya Nigam,[b]† Mohammad Aslam[c] and Dhirendra Bahadur[a*]

Among two dimensional nanomaterials, layered double hydroxides (LDH) are of great interest in biomedical applications due to their unique properties and layered structure. Superparamagnetic iron oxide nanoparticles (Fe_3O_4) are also well known for their tailorable properties, high magnetization values and biocompatibility. The objective of our current work is to combine LDH with magnetic nanoparticles in order to widen the horizons of their applications in cancer therapeutics. This work undertakes a facile chemical approach for the fabrication of Fe_3O_4-conjugated Mg-Al layered double hydroxide magnetic nanohybrids (MNHs). The successful fabrication of these MNHs was evident from X-ray diffraction, infrared spectroscopy, X-ray photoelectron spectroscopy, and zeta potential measurements. These MNHs were explored as possible heating platforms for magnetic hyperthermia as well as drug-delivery vectors to cancer cells. A high degree of drug-loading efficiency (~99%) for doxorubicin (Dox), with ~90% release under high proton environments was observed. In addition, the nature of the host-drug interactions was systematically investigated by fluorescence spectroscopy. These MNHs were seen to be biocompatible with murine fibroblast (L929) and human cervical (HeLa) cell lines. To exemplify the therapeutic performances of Dox-loaded MNHs, IC_{50} (50% inhibitory concentration) was also evaluated against HeLa cells. Calorimetric measurements revealed the specific absorption rates of 98.4 and 73.5 W/g for Fe_3O_4 and MNHs, respectively. In addition, the MNHs acted as a "cut-off switch" to maintain the hyperthermic temperature. As hyperthermia agents, these MNHs showed that a 20 min exposure to an alternating current magnetic field (ACMF) is adequate to inhibit the proliferation of HeLa cells and decrease the cell population significantly. In conclusion, the results established that these MNHs open up avenues of much more effective anticancer therapy.

Introduction

The current scenario of cancer treatment in clinical settings mainly includes radiotherapy and chemotherapy. Radiotherapy uses high-energy radiations to damage, sensitize or induce cell-cycle arrest in the cancer cells [1]. The type and quantity of radiation selected are largely based on the patient's medical condition, tumour size and region and, thus, are very carefully calculated. Classical chemotherapy in the treatment of cancer involves the use of a variety of chemicals singularly or in multitudes, in order to kill the tumour cells [2, 3]. However, both of these therapeutic approaches have generic effects, and affect the normal cells in proportions similar to cancer cells. These side effects necessitate a therapeutic alternative that can differentiate between normal and cancer cells and act selectively on the targeted tissue. Thus, the field of thermotherapy is being investigated as an alternative cure in the past few decades for cancer. Recent years have marked the development of a variety of delivery systems for various applications in therapeutics or diagnostics or both [4]. Among a vast variety of nanocarriers, superparamagnetic nanoparticles have been widely used in different biomedical applications such as drug delivery, bio-separation, immunoassay, magnetic resonance imaging and magnetic hyperthermia [5-7].

An interesting property exhibited by these superparamagnetic nanoparticles is their ability to heat up on exposure to ACMF. The heat generated by superparamagnetic nanoparticles is due to either the rotation of magnetic spins within the particle (Néel relaxation) or the rotation of the particle as a whole (Brownian relaxation) [8]. The heat dissipated during these relaxation processes is given by equation 1:

$$P = \mu_0 \chi'' \nu H^2 \qquad \textbf{(Eqn. 1)}$$

where χ" is the imaginary part of susceptibility, ν and H are the frequency and the amplitude of applied ACMF, respectively. The specific absorption rate (SAR) is the primary parameter that determines the heating capability of these nanoparticles,

[a] *Department of Metallurgical Engineering and Materials Science, Indian Institute of Technology Bombay, Mumbai, India.*
[b] *IITB-Monash Research Academy, Indian Institute of Technology Bombay, Mumbai, India.*
[c] *Department of Physics, Indian Institute of Technology Bombay, Mumbai, India.*
* Corresponding Author
† Authors have equal contribution towards this work.
Electronic Supplementary Information (ESI) available
DOI: 10.1039/x0xx00000x

and is proportional to the rate of the temperature increase [8]. This dissipated heat has been utilized in the treatment of cancer; thus, these nanoparticles are capable of performing the role of anticancer agents by themselves [9]. The interest in using superparamagnetic nanoparticles has also increased because of certain degree of possibility to be targeted to the tumour site using an external magnet (magnetic drug targeting), thereby reducing the accumulation of nanoparticles at undesired sites, as seen in other classical therapies such as chemotherapy and radiotherapy[10]. Also, high biocompatibility, biodegradability, and non-immunogenicity set these nanoparticles apart for their usefulness in magnetic hyperthermia [10, 11].

However, the continuous exposure of these nanoparticles to ACMF might lead to uncontrolled and unwanted heating, and could extend beyond the tumour boundaries, becoming detrimental to neighbouring normal tissues as well [12]. To meet this challenge, we require a material that can sense the unwanted heating and cut-off after a threshold temperature, not allowing the material to heat beyond this threshold temperature. While dealing with cancer cells, this threshold temperature window exists between 42–45 °C. A material possessing the required properties of this "cut-off switch" should have customisable architectural, chemical and physical properties, biocompatibility, biodegradability, and the ability to not generate any immunological response when present in a biological system. LDHs were thus explored as this "cut-off" in combination with magnetite as a hyperthermic entity.

LDHs are hydrotalcite-like compounds that have brucite-like positively charged layers that are balanced by counter anions and water molecules; their general formula is$[M^{2+}_{1-x}M^{3+}_{x}(OH)_2][A^{n-}_{x/n}.mH_2O]$. M^{2+} and M^{3+} are metal cations incorporated into positive layers and A^{n-} are in balancing anions present in the interlayer spacing. The high anionic exchange capability, high surface charge (readily available for binding interactions), and the biocompatible and non-immunogenic nature of LDHs have made them a prime choice as platforms in biomedical applications [13-15].Also, LDHs and their nanohybrids have been used for various applications such as controlled drug and gene delivery, catalysts, electrode materials, switchable magnetic hybrids and many more [16-19]. With regard to the toxicity of LDHs containing Al in their layers, these are less toxic to both normal and cancer cells as compared to other inorganic materials like silica, and carbon nanotubes. As observed and reported by Choy *et al*., Mg-Al LDH shows biocompatible behaviour towards many cell lines like A549, L132, HeLa and HOS[20]. These 2D nanomaterials have also been the choice for delivering a variety of drugs and nucleotide molecules establishing their biocompatibility[21, 22].

These unique physio-chemical properties, high biocompatibility, biodegradability and low-immunogenicity make Fe_3O_4 nanoparticles (magnetic) and 2-dimensional LDH (non-magnetic) stand out as potential candidates for biomedical applications. Thus, combining these nanoplatforms, might generate the required properties in addressing the challenge in the uncontrolled heating in magnetic hyperthermia. Thus, the current work demonstrates the synthesis of a hybrid material and describes the potential of LDH as the "cut-off switch", which when combined with Fe_3O_4, does not allow the temperature to rise beyond our required window [23].

Experimental

Synthesis of nanoparticles and magnetic nanohybrids

Mg-Al LDH was synthesized using a method described in previous literature, with minor modifications[24]. In brief, aqueous solution of Mg^{2+} and Al^{3+} (mole ratio 3:1) was added to0.3 M NaOH aqueous solution and stirred for 10-15 min. The white precipitate obtained was then centrifuged and washed with MilliQ water for 2-3 times. The precipitate was then re-dispersed in water and treated hydrothermally in an autoclave at 100 °C for 16 h (pressure not monitored). The LDH so obtained was washed and dried in vacuum for further studies. Citric acid-coated Fe_3O_4 nanoparticles were synthesized using our previously published work [25].Towards this end, Fe^{3+} and Fe^{2+} (mole ratio 1.9:1) were precipitated in high pH using ammonia solution at 70 °C under inert atmosphere. Citric acid was added to this solution and was incubated at 90-95 °C with mechanical stirring, inert atmosphere and reflux. The nanoparticles obtained were thoroughly washed by magnetic decantation. The Fe_3O_4 nanoparticles were then suspended in MilliQ water and sonicated to prepare a ferrofluid for further studies. The hybrid nanomaterial was prepared by simple non-covalent electrostatic interactions mediated between the cationic LDH and anionic Fe_3O_4 nanoparticles as shown in Figure 1. For this purpose, the as-prepared aqueous solutions of LDH and Fe_3O_4 nanoparticles were put in an ultrasonicator water bath for 2 h (1:1 w/w) and maintained at room temperature. These magnetic nanohybrids (MNHs) were then collected over a strong permanent magnet and then dried in vacuum at room temperature.

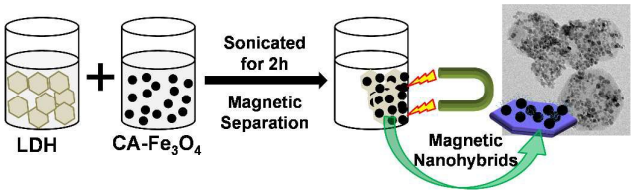

Figure 1. Schematic representation of synthesis of MNHs.

Calorimetric Measurements

Time-dependent calorimetric measurements were performed on the aqueous suspensions of MNHs to evaluate their heating efficacy, and their SAR was calculated. The ACMF was generated using an RF generator that operated at a fixed frequency (425 kHz) in a solenoidal coil with proper insulation in order to minimize heat loss. 1 ml of a colloidal suspension of Fe_3O_4 and MNHs (1, 2 and 5 mg/ml of Fe) was exposed to

ACMF with a field of 232, 271, 309, and 376Oe, and the temperature rise was recorded. The SAR was calculated using the following equation [26]:

$$SAR = C \times \frac{\Delta T}{\Delta t} \times \frac{1}{m_{Fe}} \qquad \textbf{(Eqn. 2)}$$

where, C is the specific heat of the solvent (C = C_{water} = 4.18 J/g °C), ΔT/Δt is the initial slope of the time versus temperature curve, and m_{Fe} is the mass fraction of iron in the samples. The parameters of applied ACMF, time, and the concentration of Fe were optimized to reach and maintain the suspension temperature as 45 °C for further use in hyperthermia studies.

Drug Loading and Release

Doxorubicin hydrochloride (Dox), an established anticancer agent, was used as a model drug to evaluate the potential of the MNHs as delivery vehicles. In order to determine the drug-loading efficiency and the type of interactions of drug molecules with MNHs, the fluorescence spectra of pure Dox and Dox-loaded MNHs were studied. For this purpose, different amounts of MNHs (Stock: 2 mg/ml) were added to 1 ml of an aqueous Dox solution (10µg/ml) and mixed gently for 5 min. The fluorescence spectra of the supernatant (obtained after magnetic sedimentation of drug-loaded MNHs) were then recorded. The fluorescence spectrum of 1 ml of pure DOX (10 µg/ml) was also recorded for comparative studies. The fluorescence intensities of the supernatants against that of the pure Dox solution were used to determine the loading efficiency of Dox molecules onto the MNHs. The loading efficiency (w/w %) was calculated using the following relation:

$$\%\ \textbf{Loading Efficiency} = \frac{I_{Dox} - I_S}{I_{Dox}} \times 100 \qquad \textbf{(Eqn. 3)}$$

Where I_{Dox} is the fluorescence intensity of the pure Dox solution and $I_S$is the fluorescence intensity of the supernatant. To determine the interactions between the MNHs and the Dox molecules, the fluorescence intensities were plotted against the total corresponding concentration of MNHs and analysed using the modified Stern–Volmer equation [27];

$$\log \frac{(F_0 - F)}{F} = \log K + n \log[Q] \qquad \textbf{(Eqn. 4)}$$

where F_0 and F are the fluorescence intensity of the Dox (fluorophore) in the absence and presence of MNHs (quencher), respectively, K is the binding constant, n is the binding affinity, and [Q] is the total concentration of MNHs.

The assessment of the drug release profile of the Dox-loaded MNHs was carried out under reservoir-sink conditions. For the release study, the amount of Dox-loaded MNHs was quantified according to their loading efficacy. The Dox-loaded MNHs were then magnetically decanted and re-suspended in 5 ml of a sodium acetate buffer (pH 5), and then put into a dialysis bag. The dialysis was performed against 200 ml of phosphate buffered saline (PBS; pH 7.3) under continuous stirring at 37 °C, in order to mimic the cellular environment of lysosome and cytoplasm. 1 mL aliquot of the sink (PBS) was withdrawn at fixed time intervals to be analysed for the amount of Dox released and was replaced with fresh PBS, simultaneously, to maintain the concentration gradient conditions. The aliquot was then subjected to the measurement of its fluorescence intensity, excited at 490 nm; the cumulative drug release was then calculated against the standard graph prepared under similar conditions (R^2=0.998).

***In vitro* studies**

The toxicity of a functional nanomaterial toward a biological system is an important factor that limits the use of various potential carrier materials. To meet this end, a dose-dependent viability study was performed to evaluate the biocompatibility of these MNHs with murine fibroblast cells (L929) and human cervical cancer (HeLa) cells. For a typical experiment, the cells were seeded into 96-well plates at a density of 5×10^4 cells per well for 24 h. Then, 200 µl of serial dilutions of a colloidal suspension of MNHs (2.0, 1.0, 0.5, 0.25, 0.125, 0.625, and 0.3125 mg/ml) in an appropriate supplemented growth medium were added to the cells and incubated for an additional 24 h at 37 °C in a 5% CO_2 environment. Thereafter, the cells were gently washed with PBS (pH 7.3) and then processed for the SRB assay to determine the viable cell population[28]. Non-treated cells were used as control for the experiments. For a typical assay, the cells were fixed with10% trichloroacetic acid solution by incubating at 4 °C for 1 h. The cells were then washed gently and stained by 0.4% SRB dissolved in 1%acetic acid by incubating in the dark. The cell-bound dye was then extracted with 200 µl of a 10 mM Tris buffer solution (pH 10.5), and its optical density was measured using a multi-well plate reader at 560 nm. The viable cell population was calculated as a comparative against control using the following equation:

$$\%\ \textbf{Cell Viability} = \frac{\textbf{Absorbance of treated cells}}{\textbf{Absorbance of control cells}} \times 100 \qquad \textbf{(Eqn. 5)}$$

The laser scanning confocal microscopic images were recorded to investigate the cellular internalization of the MNHs by HeLa cells. For the microscopy, the cells were seeded in a 30 mm sterile tissue culture petridish and incubated under physiological conditions (37 °C and 5% CO_2 environment) for 24h so that it could be grown as a monolayer. The cells were then incubated with the FITC-tagged MNHs that were suspended in the growth medium and incubated for a specific duration (3, 6, 12 and 24 h). Then, the cells were gently washed with PBS 3–4 times, fixed with 4% paraformaldehyde at room temperature for 10 min, and gently rinsed with PBS 3–4 times. In order to label the cell nuclei, a solution of propidium iodide (5 µg/ml in PBS) was added and incubated for 5 min, and then gently rinsed with PBS 3–4 times. They were then visualized and imaged using a confocal microscope.

Also, the amount of the internalized MNHs was determined from the inductively coupled plasma-atomic emission spectroscopic (ICP-AES) analysis of the cell lysate. HeLa cells of 5×10^4 cell density were seeded in a sterile tissue culture petridish of 30 mm and incubated

for 24 h under physiological conditions. The exhausted growth medium was then replaced by 1 mL of an aqueous suspension of MNHs (1mg/mL) that was mixed with supplemented growth medium; the cells were then incubated for 6 h under similar conditions. Subsequently, the cells were washed gently with PBS, trypsinized and suspended in 100 µl of sterile PBS. To this cell suspension, 500 µl of concentrated HCl was added and the cells were allowed to lyse for 10 min. The volume of the cell lysate was then made up to 10 ml by MilliQ water and was analysed for Fe^{2+}, Mg^{2+} and Al^{3+} ions by atomic emission spectroscopy.

The therapeutic effect of Dox-loaded MNHs was investigated using HeLa cells. To this end, 5×10^4 cells were seeded in a 96-well plate and incubated at 37 °C under 5% CO_2 environment for 24h. Thereafter, varying amounts of Dox-loaded MNHs that were suspended in a supplemented growth medium were added to the wells after replacing the exhausted growth medium. The cells were further incubated under similar conditions for an additional 24h. The SRB assay was performed to calculate the number of viable cells, as described earlier. The concentration of the Dox-loaded MNHs, which reduced the cell population by 50%, was termed as the IC_{50} value; this value plays a significant role in the determination of the therapeutic dosage.

Treatment of Cancer by Magnetic Hyperthermia

The heat-generating ability of the magnetic nanoparticles on exposure to ACMF was used in the hyperthermic treatment of the cervical cancer cells. The fatal effect of magnetic heating by the MNHs was evaluated on these cells with and without the application of ACMF. For a typical study, the HeLa cells were grown in a supplemented medium at 37 °C in a 5% CO_2 environment. After the culture reached ~90% confluency, the cells were detached from the culture flasks by treatment with a trypsin-EDTA solution, collected by centrifugation, and counted to a cell density of 1×10^6 by the trypan blue exclusion method [29]. 500µl (2 mg/ml) of sterile MNHs formulations were added to the cell suspensions and mixed gently after the volume was made up to 1 ml by the growth medium. The cell suspensions were then exposed to an ACMF of 376 Oe for initial 10 min to reach the hyperthermia temperature of 45 °C. The temperature of the suspension was maintained at 45±0.5°C; this exposure was continued for different treatment time intervals (10, 15, 20, 25 and 30 min). The selection of the applied ACMF was according to earlier optimization that was done by varying the applied field and the concentration of the MNHs. The cell suspension was then seeded in a 30 mm petridish with an additional 1 mL of supplemented growth medium and incubated for 6 h at 37 °C in a 5% CO_2 environment. The cells were then washed gently with PBS, trypsinized, and counted for viable cell population by the trypan blue exclusion method. The viable cell population was represented as under:

$$\%\ \boldsymbol{Cell\ Viability} = \frac{\boldsymbol{No.\ of\ live\ cells}}{\boldsymbol{Total\ Cells}} \times \mathbf{100} \qquad \textbf{(Eqn. 6)}$$

The treatment time at which the cancer cell population is reduced to 50% is considered to be its median lethal dose (LD_{50}).

Results and discussion

Structural Analyses

Figure 2 shows the XRD pattern of Mg-Al LDH, Fe_3O_4 nanoparticles and MNHs. While, the XRD pattern of LDH exhibited a typical rhombohedral (R-3m) hydrotalcite crystal (JCPDS: 01-089-0460), the pattern for iron oxide was indexed for a cubic inverse spinel phase of Fe_3O_4 (JCPDS: 88-0866). All the characteristic diffraction peaks of LDH and Fe_3O_4 nanoparticles were observed in the MNHs samples. It is evident from the MNHs' pattern that the peaks of Fe_3O_4 phase dominate, indicating the presence of Fe_3O_4 nanoparticles on the surface of LDH.

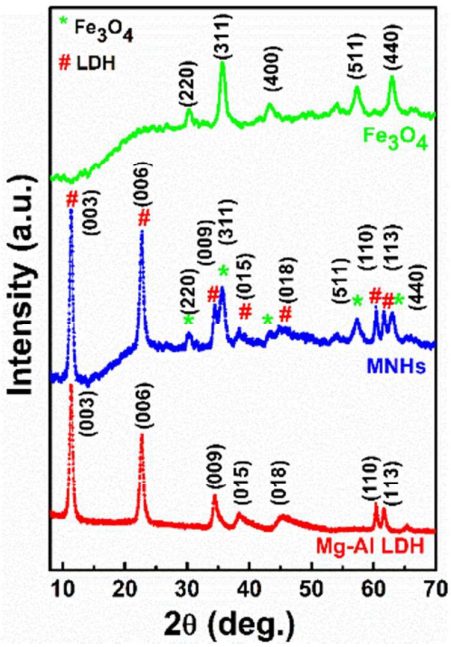

Figure 2. XRD pattern of Mg-Al LDH, Fe_3O_4 nanoparticles and MNHs

Figure 3 shows the electron micrographs of Fe_3O_4 nanoparticles, pure LDH and MNHs with their corresponding selected area electron diffraction (SAED) patterns (inset). Figure 3a shows the Fe_3O_4 nanoparticles with essentially a spherical morphology and narrow size distribution. The particles were sized in the range of 10–15 nm ($\sigma \leq 10\%$). Pure LDH (Figure 3c) shows a hexagonal morphology with nearly circular edges that has a particle size of 80–100 nm. The SAED patterns that correspond to the diffraction planes of (003), (006) and (009) were indexed. Figure 3e shows MNHs that have Fe_3O_4 nanoparticles that are well decorated and evenly distributed on the LDH surface. The SAED pattern of MNHs shows Fe_3O_4 as the primary phase and the (003) pattern of the LDH phase, which is in agreement with the XRD results.

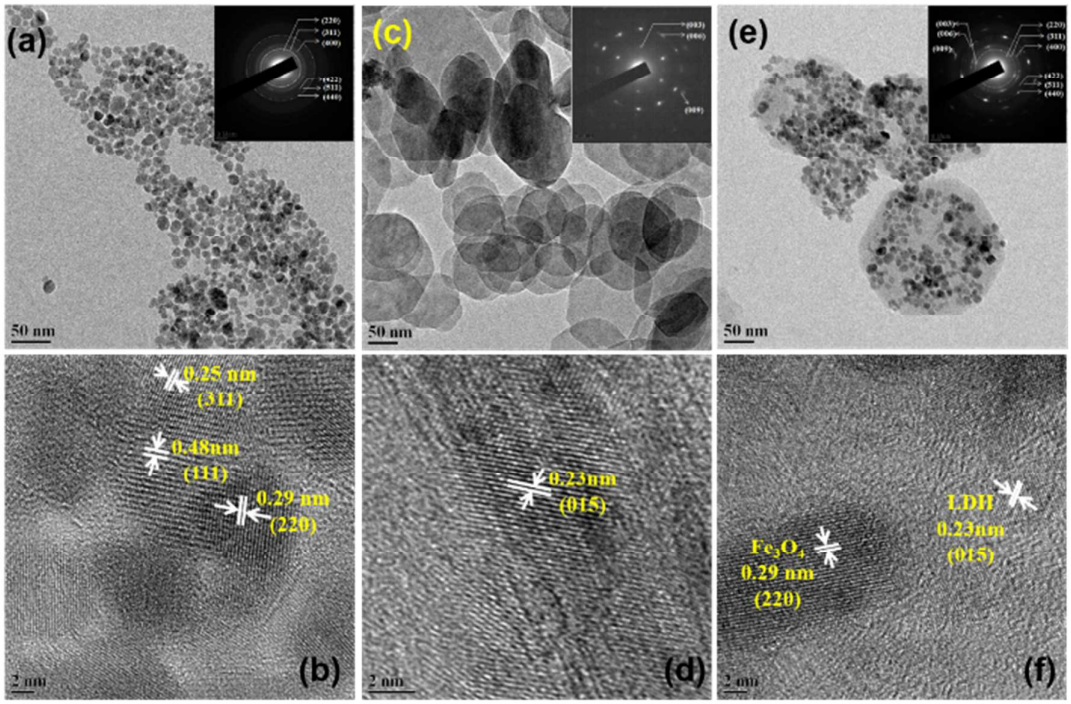

Figure 3. Transmission electron micrographs along with high resolution micrographs of (a,b) Fe_3O_4 nanoparticles, (c,d) LDH and (e,f) MNHs (Insets depict corresponding SAED patterns)

Surface Analyses

Figure 4 shows the infrared spectra of Fe_3O_4 nanoparticles, LDH and MNHs. The spectrum of Fe_3O_4 showed successful conjugation of citric acid since it had the characteristic vibrations at 3135 cm^{-1} (C-H stretching), 1601 cm^{-1} (C=O stretching), 1385 cm^{-1} (COO^- symmetric stretching), and 860–500 cm^{-1} (metal-oxygen vibrations). The evidence of carbonate intercalated in between the LDH phase is confirmed by the characteristic vibrational peaks that occur at 3553, 1646 cm^{-1} (-OH stretching), 1370 cm^{-1} ($-CO_3^{2-}$ anions) and all metal-oxygen vibrations at 800–500 cm^{-1}. The spectrum of the MNHs indicates a mixture of LDH and Fe_3O_4 phases, with a meagre shift observed in the O-H and C-H stretching bands. This shift, along with the sharp peak at 1385 cm^{-1}, indicates the attachment of Fe_3O_4 on the surface of LDH.A shoulder is seen around 3000 cm^{-1} in LDH as well as MNHs and is attributed to the hydrogen bonding between water molecules and carbonates in the interlayers of LDH sheets[30].

These nanomaterials were characterized for their hydrodynamic diameter by the dynamic light scattering (DLS) method (Figure S2). It was observed that the Fe_3O_4 nanoparticles had a size of 100±4 nm while the LDH had a size of 210±5 nm in aqueous environments with narrow size distributions. MNHs, on the other hand, had a broader size distribution with an average hydrodynamic size of 240±9 nm. These numbers play an important role when these particles are to be considered for biological applications. The hydrodynamic diameter of MNHs is seen to be almost double of its absolute size obtained from electron micrographs. The interfacial water molecules interacting with the outer charged layer of MNHs contribute to this increase in its size and also give us a better understanding of the fate of these particles *in vivo*. The poly-dispersity index for Fe_3O_4 nanoparticles, LDH and MNHs is close to 0.2 (0.18, 0.18 and 0.23 respectively). This signifies that these particles are monodisperse and form stable aqueous suspension for biological applications.

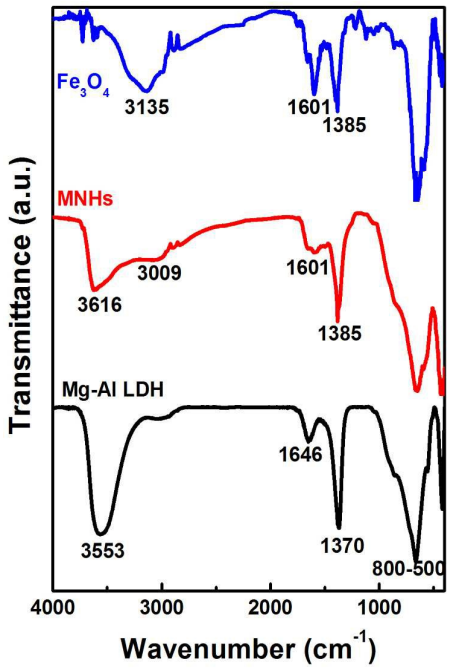

Figure 4. FTIR spectra of Mg-Al LDH, Fe_3O_4 nanoparticles and MNHs

The XPS spectra of citric acid-coated Fe_3O_4, LDH and MNHs were analysed for the C1s, O1s, Fe2p, Al2p, and Mg2p core levels. Figure 5 shows the deconvoluted core levels for the MNHs, while the spectra for citric acid-coated Fe_3O_4 and LDH are thoroughly discussed in the supplementary information. The C1s core levels were deconvoluted into three peaks that occur at 284.1, 285.3 and 288.1 eV, corresponding to the C-C, carboxylate entities and carbonates, respectively. The peaks corresponds to C-C and O-C=O occur due to the citric acid groups of Fe_3O_4, while the carbonates are present in the interlayer spacing of the LDH layered structure. The O1s levels show two deconvoluted peaks at 529.4 and 532 eV, corresponding to carboxylate-linked oxygen/hydroxide/oxide and carbonate groups, respectively. The asymmetric features seen in the spectra indicate the presence of multiple oxygen bonds. The Fe2p levels reveal the presence of $Fe2p_{3/2}$ and $Fe2p_{1/2}$ oxidation states of iron oxide. The peak that occurs at 710.2 eV corresponds to the Fe-O bonds with oxygen of citric acid, while the peaks of $Fe2p_{3/2}$ and $Fe2p_{1/2}$ occur at 712.5 and 724 eV, respectively. A small-intensity, broad peak is also seen at 718 eV, corresponding to the Fe^{3+}oxidation state of iron. The Fe2p spectra of MNHs are consistent with the spectra of the citric acid-coated Fe_3O_4 nanoparticles, indicating that the formation of MNHs has not altered the structure of Fe_3O_4 in any way. The binding energy of the Al2p core level that arises at 74.2 eV and the symmetry in the spectra suggest the existence of Al^{3+} in the hydroxide form, which corroborates well with its spectra in the pure LDH sample. The core level of Mg2p is deconvoluted into two peaks at 54.6 and 56.4 eV to conclude that Mg^{2+} is linked by both oxide/hydroxide, as well as carbonate entities. All the spectra show a shift in their binding energies, marking the successful conjugation of citric acid-coated Fe_3O_4 on to the surface of LDH layers.

The layers of the LDH sheets have the –OH groups in abundance, while the cations contribute toward their inherent positive charge. This charge-rich surface can readily interact with various nanomaterials, forming a variety of hybrid materials. This decoration of Fe_3O_4 nanoparticles on the surface of LDH is also evident by the zeta potential values of these nanomaterials. The negatively charged Fe_3O_4 and positively charged LDH are expected to interact electrostatically to form the MNHs. Zeta potential values of LDH, Fe_3O_4 and MNHs are +37.9, -26.1 and -23.9 mV, respectively, which shows a charge reversal for cationic LDH to anionic MNHs after decoration with Fe_3O_4.Most of the MNHs' surface is covered with $Fe_3O_4$with citric acid being exposed to the immediate microenvironment. This rendered a sufficiently negative zeta potential to MNHs, but slightly less in comparison to individual Fe_3O_4 nanoparticles.

Magnetic & Calorimetric Analyses

Figure 6a shows the field-dependent magnetic measurements of Fe_3O_4 and MNHs at 300 K. Fe_3O_4 nanoparticles show superparamagnetic behaviour with a magnetization value of 69.1 emu/g at an applied field of 20 KOe, which lowered after its conjugation with LDH. The LDH nanoparticles constituted the non-magnetic components in the MNHs, thereby lowering the magnetization of MNHs to 44.4 emu/g. The lowering in magnetisation of MNHs is about 36% of pure Fe_3O_4 nanoparticles. This is equivalent to the weight of LDH (~ 40%) in MNHs indicated from the elemental analysis (Table S1).The inset of the M-H curves shows negligible coercivity (~10 Oe) which is a characteristic feature of superparamagnetism. And also, ZFC-FC measurements were performed to evaluate shift in the blocking temperature (T_B), if any, of the MNHs (Figure S4). The T_B value of pure Fe_3O_4 nanoparticles and MNHs is found to be 260 and 230 K respectively and no change in the behaviour of the ZFC-FC curves was observed. This shift in T_B, for MNHs, to a lower value is due to the non-magnetic contribution of LDH and decrease in the magnetic contribution of Fe_3O_4 nanoparticles. This in turn decreases the particle-particle interaction of Fe_3O_4 nanoparticles in nanohybrids[31]. The magnetic measurements thus confirms that LDH is acting as a matrix to Fe_3O_4 nanoparticles in MNHs and are not contributing physically.

The generation of heat on exposure to an ACMF is a unique characteristic of magnetic nanoparticles owing to the Neel and Brownian relaxation losses. This property has been widely exploited by various researchers for treatment of cancer by hyperthermia [32-34].Time-dependent calorimetric measurements were performed on the aqueous suspensions of Fe_3O_4 and MNHs, and their SAR were found to be 98.4 and 73.88 W/g of Fe, respectively, at an applied field (H) of 376 Oe.

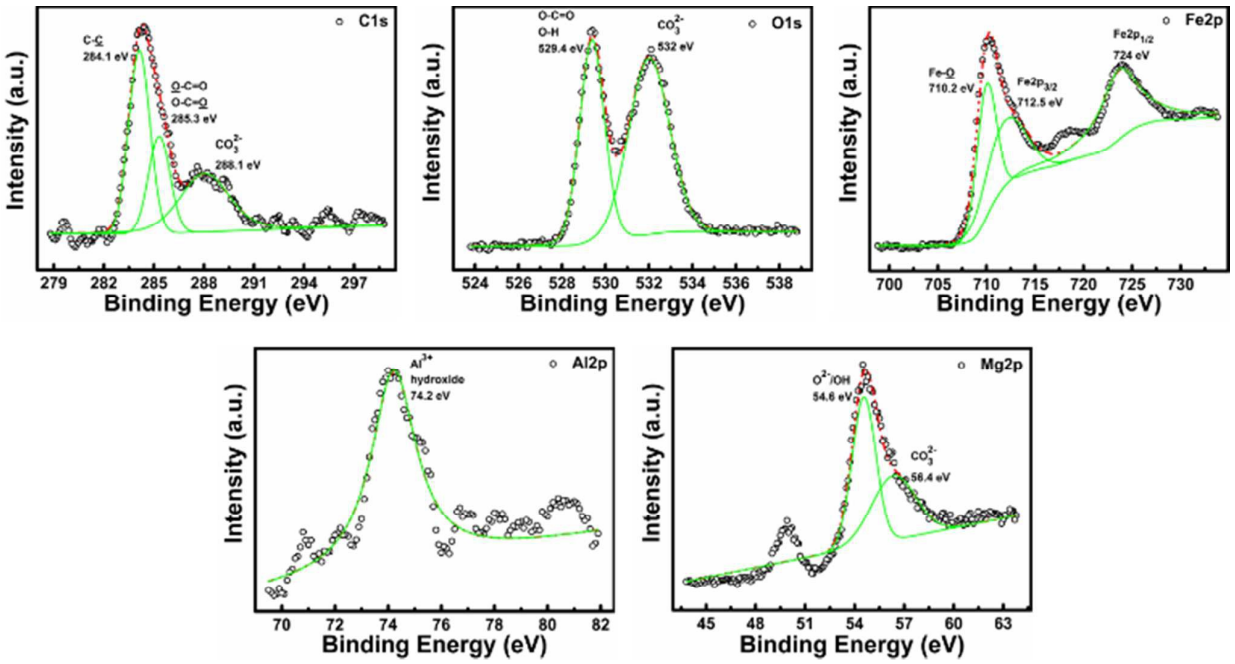

Figure 5. XPS spectra of MNHs

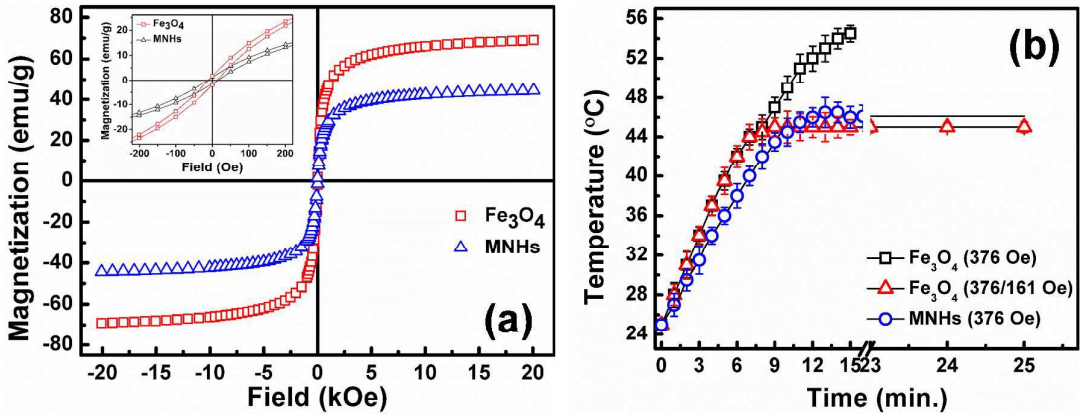

Figure 6. (a) M vs H hysteresis loops of Fe_3O_4 and MNHs recorded at room temperature with low field inset (b) Calorimetric optimization and comparative performance of Fe_3O_4 nanoparticles with MNHs

It was also observed that the time required to reach the hyperthermia temperature (45 °C) decreased with an increase in the applied field. This is in accordance with the fact that heat generation is proportional to the square of the applied ACMF (H) [35, 36]. The data efficiently establishes these MNHs as effective heating sources in hyperthermia treatment of cancer.

Figure 6b shows the optimized time versus temperature graphs used for cellular magnetic hyperthermia studies. It was seen that at an applied field of 376 Oe, citric acid-coated Fe_3O_4 nanoparticles reach 45 °C within 6-7 min, but continue to generate heat, raising the temperature of the suspension up to 55 °C, detrimental to even normal cells. This challenge was addressed by applying a combination of ACMF of varying strengths. A combination of field strengths of 376/161 Oe worked well to elevate the sample temperature to 45 °C and to maintain it for a period of approximately 25 min. On the other hand, the MNHs required the magnetic field with strength of 376 Oe for a similar performance, without any field reduction, and the MNHs acted as "cut-off switch" themselves as was required. It was observed that the MNHs reached the hyperthermia temperature within 10 min, and were capable of maintaining it for long treatment durations, making them a desirable candidate in clinical settings.

New Journal of Chemistry

ARTICLE

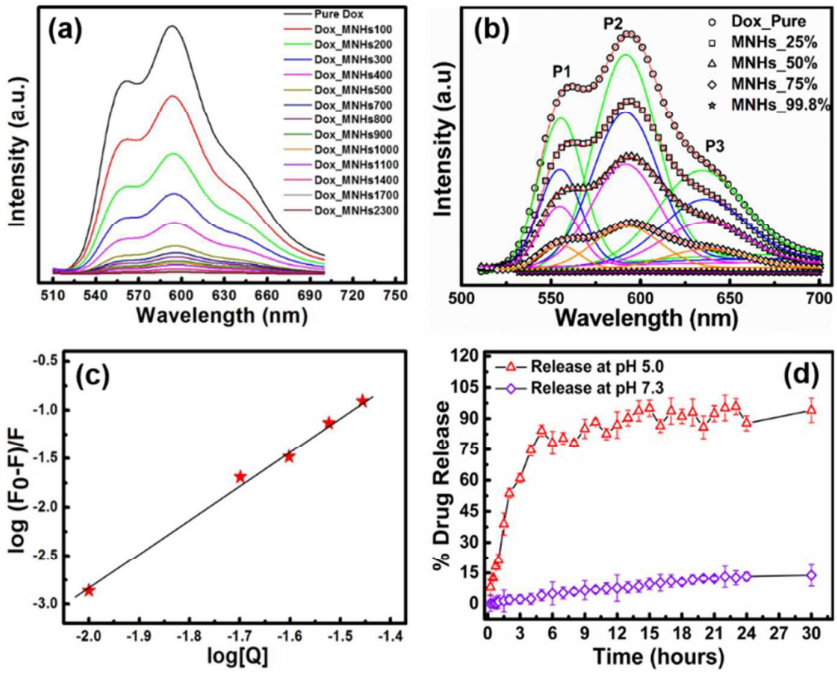

Figure 7. (a) Fluorescence spectrum of aqueous solution of pure Dox against the Dox-loaded MNHs (b) Deconvoluted Gaussian profiles at loading percentages of 25, 50, 75, and 99.8% (c) modified Stern–Volmer plot for the drug conjugation with MNHs (R^2= 0.996) (d) Cumulative Dox release profile from MNHs in the environment of pH 5.0 and 7.3 over a period of 30h

Drug loading & Release

With LDH and Fe_3O_4 being established as functional materials that are biocompatible [37, 38], the MNHs were evaluated for their capacity to carry a therapeutic payload to the desired tumour site. The fluorescence spectra of doxorubicin (Dox) were recorded to study the drug-loading efficiency of MNHs; which gave a clear picture of the interactions between Dox and MNHs. Figure 7a shows the fluorescence spectra of an aqueous solution of pure Dox against the Dox-loaded MNHs. For a constant concentration of Dox in the solution, the concentration of the MNHs was varied and a simultaneous quenching in the fluorescence was observed. Thus, it could be concluded that the increase in the concentration of the MNHs is predominantly responsible for the significant quenching of the fluorescence. Since the fluorescence intensity of any fluorophore is largely dependent on its state, that is, free or bound, this decrease in the intensity is directly attributed to the binding interactions between MNHs with the Dox and the subsequent reduction of the amount of free Dox in the solution. The positively charged $–NH_2$groups present in Dox are expected to bind electrostatically with the negatively charged carboxylate groups of citrate, which are decorated on the surface of Fe_3O_4.

Also, the presence of lone pairs of electrons on the ketone groups of Dox make them probable participating sites for the hydrogen bonding with either the citrate ions or the positively charged LDH layers, if any. The loading efficiency of MNHs was calculated to be 99.8% (w/w). The binding interactions between the Dox molecules and MNHs were further analysed and confirmed by multiple peak deconvolution by Gaussian curve fitting (Origin 8.0 software) (Figure 7b). The fluorescence spectrum of Dox exhibits three emission maxima at 560 nm (P1), 590 nm (P2), and 630 nm (P3). The nature of the Dox-MNHs interaction is signified and revealed by a change in the peak maxima position, the shape of the spectrum, and the ratios of the area under each deconvoluted peak (A1/A2 and A3/A2) [39]. In comparison with the spectrum of a pure Dox solution, a gradual decrease is observed in the values of A1/A2 and A3/A2 for the Dox-loaded MNHs, which is a clear indicative of the binding interactions between the two molecules (Table S2).

Taking a step further in the understanding of drug-MNHs interactions, the modified Stern—Volmer plot was used to calculate the binding constant of the Dox molecules to the MNHs (Figure 7c).

The data was fitted by the method of least squares with a correlation factor (R^2) of 0.996, using the Origin 8.0 software. The y-intercept of plot represents the logarithmic value of the binding constant and was calculated to be 73.36 $(mg/ml)^{-1}$ for MNHs. The slope of the plot is a representation of the binding affinity or the fraction of fluorophore taking part in the interactions with the quencher molecule (here, MNHs), which was calculated to be 3.57 (linear data fit in Origin 8.0 software). This indicates that three of the possible binding sites in Dox are utilized to form the conjugation with the MNHs. The Gibbs' free energy was calculated by the binding constant, resulting in a negative value (-11.07 kJ/mol), which indicates spontaneous binding interactions between Dox and the MNHs.

Figure 7d shows the cumulative Dox release profile from the Dox-loaded MNHs under cell-mimicking conditions over a period of 30 h. The Dox release from MNHs shows a sustained release pattern for a period of initial 5–6 h (> 50%), slowing down for the next 6h and attaining a plateau thereafter (>95%). On the other hand, at near physiological pH (7.3) the MNHs release only ~20% of the Dox even after 30 hr. The results indicate that the MNHs could efficiently release Dox molecules in high proton environments as against neutral pH environments. This difference in release percentage could be due to the decrease in the negative zeta potential of the MNHs in these acidic environments. This results in the protonation of the Dox molecules, which in turn leads to the weakening of the non-covalent binding interactions between Dox and MNHs. This weakening of the binding initiates the release of Dox into its immediate environment. This pH-stimulated drug release is desirable in cancer chemotherapeutics because the fluid surrounding the tumour cells is more acidic than the normal extracellular fluid. When the MNHs are delivered to the targeted cancer site, the release of Dox would be instigated, which would be further enhanced upon the particle internalization in the lysosomes of the cancer cells.

***In vitro* studies**

Biocompatibility and Cell Internalization Studies. The MNHs were evaluated for any toxic effects on cell proliferation or morphology of L929 and HeLa cells by incubating the cells in a medium that contained known concentrations of the MNHs. The cells without any MNHs in the growth medium were considered as control. Figure 8a shows the percentage of viable cells after treatment with the MNHs for a period of 24 h. Both L929 and HeLa cells are seen to be unaffected by the presence of MNHs in their growth medium for concentrations as high as 2 mg/mL. The cationic nature of LDH might initiate the destabilization of the plasma membrane upon contact, which is counteracted by the presence of anionic Fe_3O_4 on its surface. Also, the tolerance and survival of HeLa cells toward these MNHs could be due to the anomaly in their structure, composition and function against normal cells, which aids in their survival.

Figure 8b depicts the LSCM images captured in order to evaluate the cell internalization of the MNHs. The images show their successful internalization by HeLa cells after a period of 6h. The uptake of MNHs by these cells was seen to initiate in 3h, but the particles were scarcely internalized (data not shown), while at 6h, the MNHs marked their presence not only in the cytoplasm but some of the MNHs could also be seen in the nuclei of the cells. The internalization of the MNHs does not reveal any undesired morphological changes in the cells marking its compatibility with the HeLa cells. Green fluorescence is present due to the FITC-tagged MNHs, while the nuclei are clearly stained by propidium iodide dye (red). Also, the successful cell internalization of MNHs was supported by the results from the atomic emission spectroscopy (ICP-AES) (Figure 8c). The amount of Fe^{2+}, Mg^{2+} and Al^{3+} in the cells after 6h, when compared to the control cells that were grown without the MNHs in their growth medium, is found to be 19.0, 1.2, and 0.2 µg/mg of the MNHs, respectively.

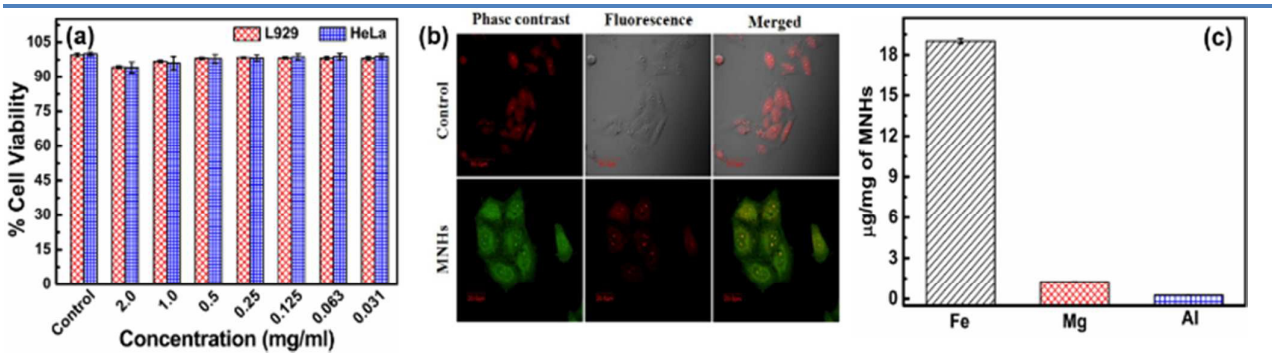

Figure 8. (a) Cell Viability after treatment of 24 h with MNHs on L929 and HeLa cells (b) LSCM images of cell internalization of MNHs after 6h and (c) ICP-AES analyses of cell lysates for the quantification of Fe^{2+}, Mg^{2+} and Al^{3+} ions.

Therapeutic Efficacy Studies. The Dox-loaded MNHs were evaluated for their therapeutic effect on HeLa cells over a period of 24 h (Figure 9a). It was observed that the concentration of 0.94 mg/mL (R^2 = 0.957) of the Dox-loaded MNHs competently reduced the viable cell population by 50% and hindered their proliferation. The IC_{50} value was calculated by the dose-responsive sigmoidal curve fitting of the Origin 8.0 software. It could, thus, be deduced that the presence of MNHs affected the IC_{50} of the Dox-loaded formulation and lowered the values when compared to the pure

Dox molecules with a similar therapeutic efficacy. Also, from the cell internalization studies performed earlier (Figure 8b) we can conclude that these MNHs are very much capable of carrying its therapeutic load inside the cells. As these MNHs are pH-sensitive (Figure 7d), a higher amount of Dox is expected to be released inside the cells in lysosomes than the amount released outside in the extracellular fluid. The Dox is then expected to diffuse from the lysosomal compartment to other parts of cell thereby showing toxic effects to the cells.

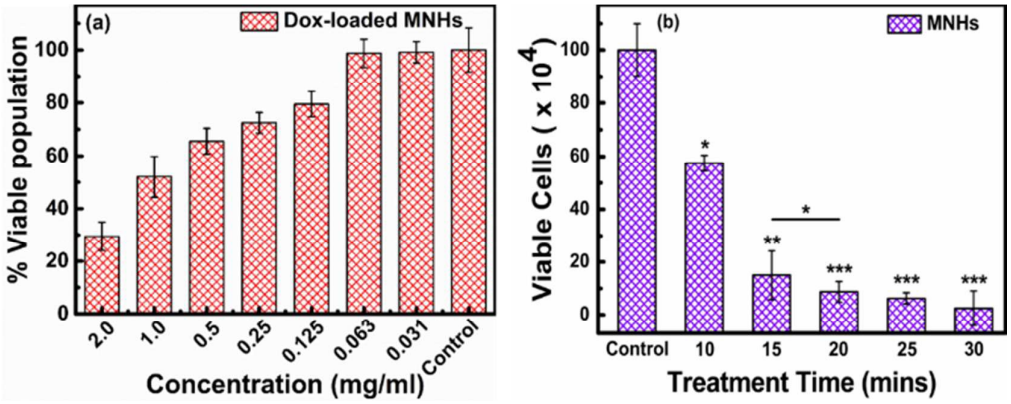

Figure 9. (a) Dose-dependent inhibition of cell proliferation of HeLa cells by Dox-loaded MNHs (IC_{50} evaluation) (b) Detrimental effects of ACMF on viability of HeLa cells in presence of MNHs (Treatment times were found to be statistically significant against control cells with $p<$ 0.05 (*), 0.01 (**) and 0.001 (***))

Treatment of Cancer by Magnetic Hyperthermia

The heat generated by the magnetic nanoparticles under the influence of an oscillating magnetic field, that is, ACMF is widely utilized for the hyperthermia treatment of cancer in *in vitro* as well as *in vivo* conditions [40, 41]. The temperature for magnetic hyperthermia is desirable between 42–45 °C where it is known to be fatal to cancer cells without being detrimental to neighbouring normal cells. Our developed MNHs were useful in elevating the temperature of the suspension from room temperature to 45 °C within 10 min of exposure to an ACMF of strength of 376 Oe (optimized earlier for different treatment times). Figure 9b depicts the effect of the applied ACMF on the viable cell population of HeLa cells. It is seen that the live cell population decreases exponentially with the increase in the treatment time. Even a small treatment time of 10 min is sufficient to reduce the number of live cells by 60% and establish the efficiency of magnetic hyperthermia. Also, this fatal effect of heat on the viability of cells attains saturation at approximately 20 min and shows minimal effect with further increase in the treatment time.

Conclusions

To conclude, the current work describes a simple facile approach for the fabrication of Fe_3O_4-decorated layered double hydroxide for use in thermo-chemo therapy of cervical cancer. These magnetic nanohybrids were thoroughly characterized and evaluated for their therapeutic efficacy. Doxorubicin was successfully loaded onto these nanohybrids, which showed an on-demand triggered release in a sustained fashion. The drug release was pH-augmented, which is a desired modality in cancer therapy due to the acidic tumour microenvironment. These carrier nanohybrids were seen to be biocompatible, with negligible toxicity. This magnetic nanohybrid platform was also assessed for its performance in the treatment of tumours by magnetic hyperthermia treatment through exposure to an AC magnetic field. The introduction of LDH in these magnetic nanohybrids acted as a "cut-off switch" for an otherwise uncontrolled heating of Fe_3O_4 nanoparticles. Overall, this newly fabricated nanohybrids platforms show promising *in vitro* results, with an enhanced therapeutic performance, and could be used to explore the combination of thermo-chemotherapy. Using magnetic nanohybrids in thermo-chemo therapy, thus, promises to be a more effective approach in the treatment of cancer against the existing classical therapies.

Acknowledgements

EVPK and SN acknowledge DST and IITB-Monash Research Academy, respectively for fellowships. The authors also acknowledge SAIF, IIT Bombay for materials characterization and Department of Physics, IIT Bombay for XPS measurements. EVPK acknowledges Department of Science and Technology for financial assistance for the current work.

References

1. G. Delaney, S. Jacob, C. Featherstone and M. Barton, *Cancer*, 2005, **104**, 1129-1137.
2. Mark A. Dawson and T. Kouzarides, *Cell*, 2012, **150**, 12-27.
3. T. Vial and J. Descotes, *Toxicology*, 2003, **185**, 229-240.
4. K. Cho, X. Wang, S. Nie, Z. Chen and D. M. Shin, *Clinical Cancer Research*, 2008, **14**, 1310-1316.

5. S. Laurent, D. Forge, M. Port, A. Roch, C. Robic, L. Vander Elst and R. N. Muller, *Chemical Reviews*, 2008, **108**, 2064-2110.
6. E. Katz and I. Willner, *Angewandte Chemie International Edition*, 2004, **43**, 6042-6108.
7. S. Chandra, K. C. Barick and D. Bahadur, *Advanced Drug Delivery Reviews*, 2011, **63**, 1267-1281.
8. R. E. Rosensweig, *Journal of Magnetism and Magnetic Materials*, 2002, **252**, 370-374.
9. Q. A. Pankhurst, J. Connolly, S. K. Jones and J. Dobson, *Journal of Physics D: Applied Physics*, 2003, **36**, R167.
10. S. Laurent, S. Dutz, U. O. Häfeli and M. Mahmoudi, *Advances in Colloid and Interface Science*, 2011, **166**, 8-23.
11. D. Ling and T. Hyeon, *Small*, 2013, **9**, 1449-1449.
12. R. Love, R. Z. Soriano and R. J. Walsh, *Cancer Research*, 1970, **30**, 1525-1533.
13. B. Zümreoglu-Karan and A. Ay, *Chem. Pap.*, 2012, **66**, 1-10.
14. A. I. Khan, L. Lei, A. J. Norquist and D. O'Hare, *Chemical Communications*, 2001, DOI: 10.1039/B106465G, 2342-2343.
15. H. S. Panda, R. Srivastava and D. Bahadur, *The Journal of Physical Chemistry B*, 2009, **113**, 15090-15100.
16. V. Rives, M. del Arco and C. Martín, *Applied Clay Science*, 2014, **88–89**, 239-269.
17. Y. Kuthati, R. K. Kankala and C.-H. Lee, *Applied Clay Science*, 2015, **112–113**, 100-116.
18. Q. Wang and D. O'Hare, *Chemical Reviews*, 2012, **112**, 4124-4155.
19. G. Abellán, C. Martí-Gastaldo, A. Ribera and E. Coronado, *Accounts of Chemical Research*, 2015, **48**, 1601-1611.
20. S.-J. Choi, J.-M. Oh and J.-H. Choy, *Journal of Inorganic Biochemistry*, 2009, **103**, 463-471.
21. B. Saifullah, P. Arulselvan, M. E. El Zowalaty, S. Fakurazi, T. J. Webster, B. M. Geilich and M. Z. Hussein, *International Journal of Nanomedicine*, 2014, **9**, 4749-4762.
22. L. Li, W. Gu, J. Chen, W. Chen and Z. P. Xu, *Biomaterials*, 2014, **35**, 3331-3339.
23. M.-Q. Zhao, Q. Zhang, J.-Q. Huang and F. Wei, *Advanced Functional Materials*, 2012, **22**, 675-694.
24. Z. P. Xu, G. S. Stevenson, C.-Q. Lu, G. Q. Lu, P. F. Bartlett and P. P. Gray, *Journal of the American Chemical Society*, 2006, **128**, 36-37.
25. S. Nigam, K. C. Barick and D. Bahadur, *Journal of Magnetism and Magnetic Materials*, 2011, **323**, 237-243.
26. M. Babincová, D. Leszczynska, P. Sourivong, P. Čičmanec and P. Babinec, *Journal of Magnetism and Magnetic Materials*, 2001, **225**, 109-112.
27. B. Ahmad, S. Parveen and R. H. Khan, *Biomacromolecules*, 2006, **7**, 1350-1356.
28. V. Vichai and K. Kirtikara, *Nat. Protocols*, 2006, **1**, 1112-1116.
29. W. Strober, in *Current Protocols in Immunology*, John Wiley & Sons, Inc., 2001.
30. T. HIBlNO, Y. YAMASHITA, K. KOSUGE and A. TSUNASHIMA, *Clays and Clay Minerals*, 1995, **43**, 427-432.
31. K. Rumpf, Petra Granitzer, P. M. Morales, P. Poelt and M. Reissner, *Nanoscale Research Letters*, 2012, **7**, 1-4.
32. K. Hayashi, K. Ono, H. Suzuki, M. Sawada, M. Moriya, W. Sakamoto and T. Yogo, *ACS Applied Materials & Interfaces*, 2010, **2**, 1903-1911.
33. M. N. Luwang, S. Chandra, D. Bahadur and S. K. Srivastava, *Journal of Materials Chemistry*, 2012, **22**, 3395-3403.
34. M. Johannsen, B. Thiesen, P. Wust and A. Jordan, *International Journal of Hyperthermia*, 2010, **26**, 790-795.
35. Y. Piñeiro-Redondo, M. Bañobre-López, I. Pardiñas-Blanco, G. Goya, M. A. López-Quintela and J. Rivas, *Nanoscale Research Letters*, 2011, **6**, 383-383.
36. P. de la Presa, Y. Luengo, M. Multigner, R. Costo, M. P. Morales, G. Rivero and A. Hernando, *The Journal of Physical Chemistry C*, 2012, **116**, 25602-25610.
37. S. J. Choi, J. M. Oh and J. H. Choy, *J Nanosci Nanotechnol*, 2010, **10**, 2913-2916.
38. Y. Liu, Z. Chen and J. Wang, *Journal of Nanoparticle Research*, 2011, **13**, 199-212.
39. K. C. Barick, S. Nigam and D. Bahadur, *Journal of Materials Chemistry*, 2010, **20**, 6446-6452.
40. T.-J. Li, C.-C. Huang, P.-W. Ruan, K.-Y. Chuang, K.-J. Huang, D.-B. Shieh and C.-S. Yeh, *Biomaterials*, 2013, **34**, 7873-7883.
41. T. Sadhukha, T. S. Wiedmann and J. Panyam, *Biomaterials*, 2013, **34**, 5163-5171.

In-vitro Evaluation of Layered Double Hydroxide-Fe_3O_4 Magnetic Nanohybrids for Thermo-Chemo Therapy

EswaraVara Prasadarao Komarala,[a†] Saumya Nigam,[b†] Mohammad Aslam[c] and Dhirendra Bahadur[a*]

[a]Department of Metallurgical Engineering and Materials Science, Indian Institute of Technology Bombay, Mumbai, India

[b]IITB-Monash Research Academy, Indian Institute of Technology Bombay, Mumbai, India

[c]Department of Physics, Indian Institute of Technology Bombay, Mumbai, India

Graphical Abstract

Combining layered double hydroxides with Fe_3O_4 nanoparticles resulted in the desired "cut-off switch" for threshold temperature towards magnetic hyperthermia.